Isotopic Mass and Lattice Constant: X-ray Standing Wave Measurements

Alexander Kazimirov, Jörg Zegenhagen,* Manuel Cardona

The molecular volume of crystals depends on their isotopic masses. This influence originates from the zero-point motion and the resulting small differences in lattice constants. This effect was measured with high precision by using an x-ray standing wave. The standing wave is generated during Bragg reflection and thus is in phase with the planes of the substrate crystal, which is covered with a homoepitaxial film that has a different isotopic composition than the substrate. The positions of the surface planes of the film with respect to the substrate planes are revealed by the photoelectrons excited by the maxima of the standing wave. For germanium-76 on natural germanium(111), a difference in lattice constant of -1.1×10^{-5} and -2.5×10^{-5} at 300 and 54 kelvin, respectively, was found. The results are in good agreement with theoretical predictions.

The availability of materials that are highly enriched isotopically has prompted investigations of the effect of the isotopic composition on various properties such as the electronic band structure and the lattice dynamics of solids (*1*). Isotopic composition also affects basic characteristics such as the density and other structural parameters. The isotopic effect on the lattice parameters is largest at low temperatures, resulting from the effect of the nuclear masses on the zero-point vibrations and the related anharmonicity (*2*). It is thus one of the few consequences of quantum mechanics that can be unveiled by careful macroscopic observations.

Since the early work of London (*2*), a few theoretical papers have been published recently on the issue of lattice constant versus isotopic mass, such as ab initio calculations of the isotopic effect for carbon, silicon, and germanium based on density-functional perturbation theory (*3*). The local-density approximation perturbation approach was applied to the study of the isotopic effect in compound semiconductors (*4*), which gave results similar to those obtained with semiempirical methods (*5*). Recently, path-integral Monte-Carlo simulations were used to calculate the lattice constants of different crystalline germanium isotopes (*6*).

The differences in lattice constant caused by isotopic composition are usually proportional to the relative mass difference ($\approx \Delta M/M$) and vanish above the Debye temperature; at 100 K, the expected (*3*) relative change in lattice parameter between natural Ge (M = 72.59) and ^{76}Ge, expressed as $(^{76}a - {}^{nat}a)/{}^{nat}a = \Delta a/a$, is about 2×10^{-5}. Accurate measurement of such a small difference is not possible with standard diffraction techniques. There are only very few experimental data available from studies that used modified diffraction techniques and almost perfect single crystals.

The lattice constants of diamond have been determined for different isotopic compositions (*7*). Despite the fact that the measurements were done at room temperature only, with error bars in $\Delta a/a$ of about 2×10^{-5}, the isotopic effect could be observed because it is comparably large for diamond due to its high Debye temperature and small average mass. The difference in lattice constant between a natural and an isotopically enriched ^{74}Ge crystal at 300 and 78 K was measured with an elaborate, specially designed three-axis diffractometer (*8*). However, controlling all possible sources of error proved difficult, and the margin of error was considerably underestimated. As shown further below, the obtained results were not in agreement with the calculations mentioned above and led to difficulties in the interpretation of other experiments (*9, 10*).

In a different approach we used the interference field, generated inside a Ge(111) substrate crystal of natural isotopic composition, as a basis to measure the shift of the surface of an epitaxial overlayer of ^{76}Ge that is caused by the cumulative lattice constant difference of the more than 4000 lattice planes of the 1.36-μm-thick ^{76}Ge film. In this way, the interference field, generated by the Ge crystal of natural isotopic composition and therefore periodic with the substrate lattice, serves as a precise benchmark for the lattice positions of the surface layers of the ^{76}Ge overlayer (Fig. 1A). This approach has several advantages. With molecular beam epitaxy in ultrahigh vacuum, an ultraclean overlayer of high perfection can be prepared without the need for large amounts of the desired isotope (*11*). Furthermore, because the lattice mismatch at the growth temperature is extremely small, and the film grows in a truly pseudomorphic manner, the overlayer will be tetragonally distorted upon cooling down, and thus the difference in lattice constant in the direction normal to the surface [here (111)] will be enhanced [here by a factor of 1.37 (*12*)] as determined by the elastic constants.

During Bragg diffraction, an x-ray standing wave (XSW) field is generated within the overlap region of the incident and reflected x-ray waves. The periodicity of the XSW matches the

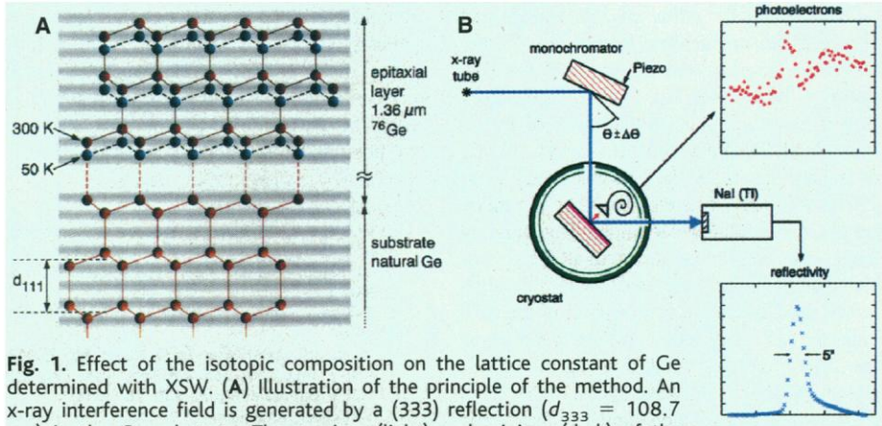

Fig. 1. Effect of the isotopic composition on the lattice constant of Ge determined with XSW. (**A**) Illustration of the principle of the method. An x-ray interference field is generated by a (333) reflection (d_{333} = 108.7 pm) in the Ge substrate. The maxima (light) and minima (dark) of the wavefield are in phase with the atomic planes (d_{111} = 326.2 pm) of the substrate (light red) and serve as a means to measure the shift of the positions of the atomic planes of the outer layers of a homoepitaxial film of ^{76}Ge (darker red) at room temperature and at low temperature (blue). The shift at low temperature has been exaggerated by a factor of 2 for clarity. Indicated is the wavefield location for the low glancing angle (Θ) side of the Bragg reflection. Traversing the total reflection range, the wavefield moves inward by half the wavefield spacing, that is by 54 pm, and gives rise to a maximum of photoemission when its maxima pass the location (center) of the Ge atoms. (**B**) The experimental setup. The intensities of the reflected x-rays and photoelectrons are recorded by a NaI(Tl) detector and a channeltron, respectively, as a function of the glancing angle of the monochromator. The reflecting planes of monochromator and sample are indicated in red.

Max-Planck-Institut für Festkörperforschung Heisenbergstrasse 1, D-70569 Stuttgart, Germany.

*To whom correspondence should be addressed. E-mail: jorg@tunux2.mpi-stuttgart.mpg.de

periodicity of the diffraction planes d_{hkl}. If the Bragg diffraction region is traversed by varying the glancing angle starting from the low-angle side, the phase of the reflected wave shifts by 180°, and as a result the XSW pattern moves inward by one-half of d_{hkl} (*13*). The measurement of the concomitant angular dependence of the photoexcitation of atoms within the range of the XSW by spectroscopic techniques provides the possibility of locating these atoms with respect to the host lattice. This technique, known as the XSW method (*14*), has matured during the last two decades into a powerful tool for surface and interface structural analysis (*15*).

The yield of photoelectrons excited by the XSW from a single layer of atoms on the surface of a Bragg-reflecting crystal as a function of the glancing angle Θ is given by (*15*)

$$Y^{hkl}(\Theta) = 1 + R(\Theta) + 2\sqrt{R(\Theta)}\cos[v(\Theta) - 2\pi P]$$

where $R(\Theta)$ is the reflectivity, $v(\Theta)$ the phase of the Bragg reflected wave, and $P = z_a/d_{hkl}$ where z_a gives the position of the atom normal to the (hkl) diffraction planes with spacing d_{hkl}. For the lattice atoms of a homogeneous crystal, $P = 0$ ($z_a = 0$) and the yield curve shows a characteristic minimum and maximum at the low- and high-angle side of the reflectivity curve, respectively. However, for the homoepitaxial Ge layer of thickness t with a very small relative lattice constant difference in the direction normal to the diffraction planes of $\Delta d_\perp/d_\perp$, the surface atoms of the film are shifted by $t \times \Delta d_\perp/d_\perp$, and thus $P = t \times (\Delta d_\perp/d_\perp)/d_{hkl}$. To determine this phase shift P, we detect photoelectrons and are therefore integrating over a small depth because of the short mean free path of the photoelectrons (*16*).

The experimental setup is shown schematically in Fig. 1B. For the XSW measurements we used a double-crystal diffractometer with a horizontal scattering geometry. Copper-K_α radiation from a stationary anode of a 1.5-kW x-ray generator was selected and slightly collimated by a Ge(333) monochromator crystal that was mounted on a microgoniometer. The crystal was scanned in Θ by a piezotransducer, thus scanning the Ge(333) rocking curve of the sample, which was mounted on a He flow-through cryostat for the XSW measurements. Photoelectrons were detected at a grazing exit angle of 0° to ~15° with the help of a channeltron. A diode temperature sensor was mounted close to the sample for an accurate determination of the sample's temperature. The intensity of the (333) Bragg reflection from the sample was monitored by a scintillation detector and used as a reference signal for drift correction during the measurements, which were performed in a signal-averaging mode (*17*). With a typical photoelectron count rate of about 1 to 2 cps, the XSW measurement at a given temperature took 10 to 20 hours and involved 3000 to 5000 scans.

In a set of experimental photoelectron yield curves measured from room temperature (T = 301 K) down to 54 K (Fig. 2), changes in the shape of the curves can be distinguished. At 301 K, a maximum of the photoelectron yield (arrows in Fig. 2) is observed on the right-hand (high-angle) side. It gradually disappears as the temperature is lowered to 150 K but shows up again at the left (low-angle) side upon further cooling to T = 54 K. This change in the shape of the yield curves is due to the inward contraction of the outermost layers of the ^{76}Ge film with respect to the wavefield and thus to the lattice spacing of the substrate upon cooling as schematically indicated in Fig. 1A. At room temperature, the maxima of the wavefield, which move inward as a function of Bragg angle, reach the atomic planes of the outer layers of the ^{76}Ge film just at the rightmost side of the range of total reflection. As the whole ^{76}Ge film contracts with decreasing temperature, these planes are not reached by the wavefield maxima any longer. At 150 K the maximum at the high-angle side of the photoelectron yield curve has disappeared. However, as the ^{76}Ge film contracts further with further decreasing temperature, the maxima of the wavefield meet the atomic planes of the ^{76}Ge surface layers already at the low-angle side, leading correspondingly to a pronounced maximum in the photoelectron yield curve at 54 K. Apparently, from the highest to the lowest temperature, the ^{76}Ge atoms at the sample surface shift inward by about the distance the wavefield maxima traverse with angle, that is, by about half of d_{333} = 109 pm.

The dynamical theory of x-ray diffraction (*13*) is needed for an accurate analysis of the XSW data and to fit the experimental photoelectron yield curves (*18*). Only the lattice mismatch $\Delta d_\perp/d_\perp$ is used as a free parameter. To obtain the unstrained lattice constant difference of the ^{76}Ge isotope versus natural Ge, we used the relation between the lattice strain parallel and perpendicular to (111), that is $e_\parallel$ and $e_\perp$, respectively, as given by elasticity theory. Thus, we multiplied $\Delta d_\perp/d_\perp$ with the quantity $e_\parallel/(e_\perp - e_\parallel)$ obtained from elastic constants reported for Ge (*12*). The resulting temperature dependence of the relative lattice constant difference $\Delta a/a$ (Fig. 3) is compared with previous experiments and calculations, rescaled to our mass difference ΔM = 3.05. An interpolation given in (*3*) and reproducing those calculated data with an error of 2% is shown as a solid line. Our experiments agree well with the theoretical data of (*3*). The deviation is much smaller than the ~10% difference between the two theoretical studies. In contrast, the older measurements of (*8*), in particular for 78 K, yielded a much larger difference in lattice constant. The precision of the method used in the present study, with an uncertainty in $\Delta a/a$ of 8×10^{-7} at 300 K, is determined by the 7% error in the thickness measurement of the ^{76}Ge film. This can be further improved to yield even more accurate values for the lattice mismatch and, we suggest, can be efficiently applied to study isotopic effects in other crystalline materials such as compound semiconductors (*5*).

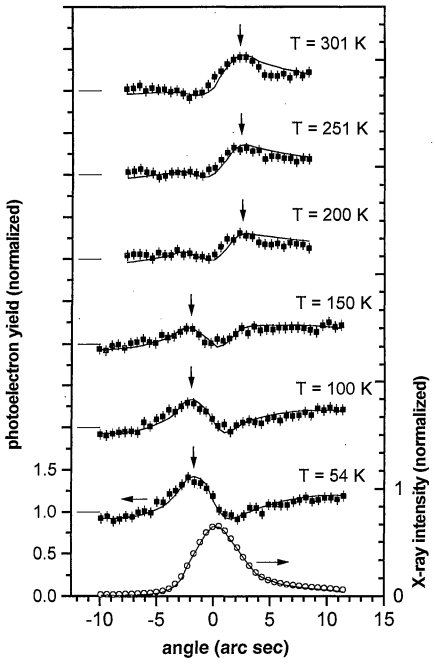

Fig. 2. Ge(333) reflectivity and photoelectron yield from the epitaxial ^{76}Ge layer as a function of the glancing angle Θ for different temperatures. The solid lines are fits to the experimental data (symbols). The fit to the reflectivity determines the angular scale and fits to the photoelectron signal yield determine the surface phase shifts P.

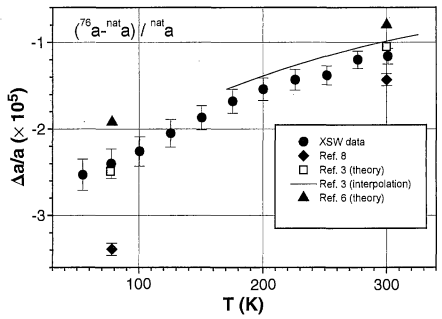

Fig. 3. Lattice constant difference between natural Ge and ^{76}Ge versus temperature. Shown are the results of the present measurement and, for comparison, the experimental results of (*8*) and the results of the calculations of (*3*) and (*6*), all scaled to our mass difference.

References and Notes

1. M. Cardona, in *Advances in Solid State Physics*, R. Helbig, Ed. (Vieweg, Braunschweig/Wiesbaden, Germany, 1994), vol. 34, pp. 35–50.

2. H. London, *Z. Phys. Chem.* **16**, 302 (1958).
3. P. Pavone and S. Baroni, *Solid State Commun.* **90**, 295 (1994).
4. A. Debernardi and M. Cardona, *Phys. Rev. B* **54**, 11305 (1996).
5. N. Garro *et al.*, *ibid.*, p. 4732.
6. J. C. Noya, C. P. Herrero, R. Ramírez, *ibid.* **56**, 237 (1997).
7. H. Holloway, K. C. Hass, M. A. Tamor, T. R. Anthony, W. F. Banholzer, *ibid.* **44**, 7123 (1991).
8. C. Buschert, A. E. Merlini, S. Pace, S. Rodriguez, M. H. Grimsditch, *ibid.* **38**, 5219 (1988).
9. C. Parks, A. K. Ramdas, S. Rodriguez, K. M. Itoh, E. E. Haller, *ibid.* **49**, 14244 (1994).
10. S. Zollner, M. Cardona, S. Gopalan, *ibid.* **45**, 3376 (1992).
11. The epitaxial film of the highly enriched ^{76}Ge isotope (average mass 75.63) was grown on an intrinsic Ge(111) substrate in an ultrahigh vacuum system (base pressure 10^{-11} mbar) by molecular beam epitaxy at a substrate temperature of 720 K, well below the threshold for bulk interdiffusion [H. D. Fuchs *et al.*, *Phys. Rev. B* **51**, 16817 (1995)]. Before and after the growth of the sample, reference films were grown and their thickness was measured with a step stylus to calibrate the growth rate, which was 1.0 ± 0.07 nm/min, as also found by a quartz microbalance. The thickness of the film is determined by the duration of growth.
12. J. Honstra and W. J. Bartels, *J. Cryst. Growth* **44**, 513 (1978).
13. M. v. Laue, *Röntgenstrahlinterferenzen* (Akademische Verlagsgesellschaft, Frankfurt/Main, 1960).
14. B. W. Batterman, *Phys. Rev. A* **133**, 759 (1964).
15. J. Zegenhagen, *Surf. Sci. Rep.* **18**, 199 (1993).
16. For the escape depth of the Ge-L photoelectrons, we used μ^{-1} = 59 nm calculated by Kovalchuk *et al.* [M. V. Kovalchuk, D. Liljequist, V. G. Kohn, *Sov. Phys. Solid State* **28**, 1918 (1986)] by Monte Carlo simulation.
17. A. Krolzig, G. Materlik, J. Zegenhagen, *Nucl. Instrum. Methods* **208**, 613 (1983).
18. We used an algorithm proposed by Kohn [V. G. Kohn and M. V. Kovalchuk, *Phys. Stat. Sol.* **A64**, 359 (1981)] based on the Takagi-Taupin equations using recurrent relations for the amplitude ratio E_h/E_0 of reflected and incident wave and the intensity of the refracted wave $I_0 = |E_0|^2$ to calculate the total field distribution in the semi-infinite sample and the epitaxial overlayer with a different lattice constant. By fitting the curve for the lowest temperature (T = 54 K), the static Debye-Waller factor of the film was determined to be e^{-W} = 0.76, which was used with the thermal Debye-Waller factors for germanium [B. W. Batterman and D. R. Chipman, *Phys. Rev.* **127**, 690 (1962)] for fitting all experimental data.
19. We are grateful to V. Kohn for the computer code for the analysis based on the Takagi-Taupin equation, to K. Eberl and E. Gmelin for valuable discussions, and to W. Stiepany, P.-Y. Lowys, G. Schneider, T. Chaperon, M. Siemers, and A. Riccardi for technical assistance.

7 July 1998; accepted 24 September 1998

Spontaneous Emission Spectrum in Double Quantum Dot Devices

Toshimasa Fujisawa, Tjerk H. Oosterkamp, Wilfred G. van der Wiel, Benno W. Broer, Ramón Aguado, Seigo Tarucha, Leo P. Kouwenhoven*

A double quantum dot device is a tunable two-level system for electronic energy states. A dc electron current was used to directly measure the rates for elastic and inelastic transitions between the two levels. For inelastic transitions, energy is exchanged with bosonic degrees of freedom in the environment. The inelastic transition rates are well described by the Einstein coefficients, relating absorption with stimulated and spontaneous emission. The most effectively coupled bosons in the specific environment of the semiconductor device used here were acoustic phonons. The experiments demonstrate the importance of vacuum fluctuations in the environment for quantum dot devices and potential design constraints for their use for preparing long-lived quantum states.

Electronic quantum devices allow the quantum mechanical properties of electrons confined to small regions in a solid to be explored. Existing devices include semiconductor resonant tunneling diodes (*1*) (based on quantum mechanical confinement), superconducting Josephson junction circuits (*2*) (based on macroscopic phase coherence), metallic single-electron transistors (*3*) (based on quantization of charge), and molecular electronic devices (*4*). The principle of operation in circuits of these devices is based on controlling energy states, for instance, by means of an external (gate) voltage. Thermal energy is always a source for unwanted transitions and errors. Even at zero temperature, however, vacuum fluctuations in the environment can give rise to transitions between states of nonequal energy by spontaneous emission of an energy quantum. Such inelastic transitions cause errors in many proposed schemes for quantum circuits. Here we studied inelastic transitions in a fully controllable, two-level quantum system realized in a double quantum dot device. We can relate the transition rates involving emission to absorption rates by the Einstein coefficients over the full energy and temperature range we studied. At the lowest temperature (23 mK), we directly measured the energy-dependent rate for spontaneous emission and determined that, in our specific semiconductor device, this energy is emitted into the environment formed by acoustic phonons.

Our double quantum dot (Fig. 1A) is fabricated in the two-dimensional electron gas (2DEG) of an AlGaAs-GaAs semiconductor heterostructure (*5*). The source and drain are large 2DEG regions that serve as leads for contacting current and voltage wires. The two dots, L and R, are separated from each other and from the leads by potential barriers induced by negative voltages applied to the three metallic gates. Tunneling between the different regions is sufficiently strong to detect current but weak enough that the number of electrons in each dot is a well-defined integer. The energy states in such fully confined regions are discrete, 0D states, resembling discrete atomic states (*6, 7*). The discrete energies include contributions from single-electron charging energies (arising from Coulomb interactions) and from quantum-mechanical confinement. The lowest energy state for one additional electron in the L dot is labeled in Fig. 1, B to D, as E_L, and similarly E_R for the R dot. Figure 1C illustrates the resonance condition, $E_L = E_R$, in which case an electron can tunnel elastically from an occupied state in the source via E_L and E_R to an empty state in the drain. Such tunneling sequences of single electrons are regulated by the Coulomb charging energies (*3, 7*). When the two states are not aligned, $E_L \neq E_R$, only inelastic transitions are allowed for which some energy needs to be exchanged with the environment. A measured off-resonance current, therefore, directly provides information about the coupling between electrons on the dots to degrees of freedom in the environment. The inelastic rates can be analyzed with well-developed methods in quantum optics (*8, 9*).

A typical current spectrum versus $\varepsilon \equiv E_L - E_R$ at our lowest lattice temperature T = 23 mK (*10*) is shown in Fig. 1E. The gate voltages V_{GR} and V_{GL} are swept simultaneously such that the respective energies are like those illustrated in Fig. 1, B to D; that is, ε = 0 occurs in the middle between the Fermi energies of source and drain, μ_S and μ_D, and $|\varepsilon| = eV_{SD}$ (its maximum) corresponds to having the states E_L and E_R aligned to one of the Fermi energies. To analyze the large asymmetry, we decomposed the total current $I_{tot}(\varepsilon) = I_{el}(\varepsilon) + I_{inel}(\varepsilon > 0)$ into a symmetric part $I_{el}(\varepsilon) = I_{el}(-\varepsilon)$ (dashed curve) and the remaining asymmetric part $I_{inel}(\varepsilon > 0)$ (dotted-dashed curve). At T = 0, $I_{el}(\varepsilon)$ is due

T. Fujisawa, Department of Applied Physics and DIMES, Delft University of Technology, 2600 GA Delft, Netherlands, and NTT Basic Research Laboratories, 3-1, Morinosato-Wakamiya, Atsugi, Kanagawa, 243-0198, Japan. T. H. Oosterkamp, W. G. van der Wiel, B. W. Broer, R. Aguado, L. P. Kouwenhoven, Department of Applied Physics and DIMES, Delft University of Technology, 2600 GA Delft, Netherlands. S. Tarucha, NTT Basic Research Laboratories, 3-1, Morinosato-Wakamiya, Atsugi, Kanagawa, 243-0198, Japan, and Department of Physics, University of Tokyo, 7-3-1 Hongo, Bunkyo-ku, Tokyo 113-0033, Japan.

*To whom correspondence should be addressed. E-mail: leo@qt.tn.tudelft.nl